Published in final edited form as:
*Nature*. 2019 November ; 575(7784): 704–710. doi:10.1038/s41586-019-1768-0.

# Mechanism of head-to-head MCM double-hexamer formation revealed by cryo-EM

**Thomas CR Miller**[1], **Julia Locke**[1], **Julia F Greiwe**[1], **John FX Diffley**[2], **Alessandro Costa**[1]

[1]Macromolecular Machines Laboratory, The Francis Crick Institute, NW1 1AT, London, UK

[2]Chromosome Replication Laboratory, Francis Crick Institute, NW1 1AT, London, UK

## Abstract

In preparation for bidirectional replication, the origin recognition complex (ORC) loads two MCM helicases forming a head-to-head double hexamer (DH) around DNA[1,2]. How DH formation occurs is debated. Single-molecule experiments suggest a sequential mechanism whereby ORC-dependent loading of the first hexamer drives second hexamer recruitment[3]. In contrast, biochemical data show that two rings are loaded independently via the same ORC-mediated mechanism, at two inverted DNA sites[4,5]. We visualized MCM loading using time-resolved EM, to identify DH formation intermediates. We confirm that both hexamers are recruited via the same interaction between the MCM and ORC C-terminal domains, and identify the mechanism for coupled MCM loading. A first loaded hexamer locked around DNA is recognized by ORC, which unexpectedly engages the N-terminal homo-dimerization interface of MCM. In this configuration, ORC is poised to direct second hexamer recruitment in an inverted orientation, suitable for DH formation. Our data reconcile two apparently contrasting models.

## Introduction

Genome replication in eukaryotes is tightly controlled to ensure that chromosomes are copied only once per cell cycle. Before cells enter S phase, two copies of an MCM hetero-hexameric helicase are loaded onto duplex DNA forming a double hexamer (DH)[1,2,6,7]. DHs mark origin DNA that can support replisome assembly and, once activated, the MCMs unwind DNA providing the template for replicative polymerases to perform bidirectional replication. Inhibiting DH formation is a major pathway for preventing re-replication and



Correspondence to Alessandro Costa (alessandro.costa@crick.ac.uk).

**Author contributions**

TCM and AC conceived the study. TCM designed biochemistry experiments. TCM, JG and JL prepared biochemical reagents and developed the assays. TCM, JG and JL performed negative stain imaging. TCM and JL performed cryo-EM imaging. TCM performed all image processing/atomic model building and developed the ReconSil reconstitution method. JFXD provided reagents. AC supervised the study. TCM and AC wrote the manuscript with input from JFXD and the other authors.

**Competing interests**

The authors declare no competing financial interests.

**Data availability**

Cryo-EM map and atomic model coordinates for the MO complex are deposited in the Electron Microscopy Data Bank and Protein Data Bank respectively under the accession code 6RQC and EMD-4980.


Europe PMC Funders Author Manuscripts

maintaining genome stability[8,9]. MCM loading requires *i.* DNA association of the origin recognition complex (ORC) and Cdc6, *ii.* opening of a DNA gate in MCM (stabilized by Cdt1[1,2,10,11]), and *iii.* ATP hydrolysis by MCM to close the gate around DNA[12,13].

A model for loading a first MCM helicase onto DNA has been proposed on the basis of biochemical[4,14], single-molecule[15] and cryo-electron microscopy (EM) analysis[10,11,16,17]. ORC first encircles and bends origin DNA[18]. Upon Cdc6 and then MCM recruitment, ORC threads the double helix through the DNA gate of MCM (between Mcm2 and Mcm5), leading to the formation of an ORC-Cdc6-Cdt1-MCM (OCCM) intermediate that encircles DNA[17–19]. In this complex, the C-terminal face of an ORC-Cdc6 ring engages the C-terminal face a notched MCM ring. Notably, OCCM has been observed in the presence of a slowly hydrolysable ATP analogue that allows MCM recruitment to DNA, but not the hydrolysis dependent MCM ring closure required to complete loading[4,14,17].

The mechanism for second MCM ring recruitment and DH formation is debated. According to a single-molecule study from the Bell group, the first MCM ring is loaded by one ORC complex and then drives recruitment of the second ring[3]. However, biochemical evidence shows that the same elements in MCM are required for recruiting both the first and second rings[4]. Combined with the observation that two inverted ORC binding sites promote efficient MCM loading[5], these data support a model whereby two distinct ORC-DNA engagement events symmetrically load two MCM rings via the same mechanism. Explaining head-to-head DH formation is critical for understanding how the symmetry of bidirectional replication is established.

## In silico reconstitution of helicase loading using single-particle EM images

To elucidate the steps that lead to DH formation, we took an EM approach to visualize the entire, ATPase dependent MCM loading reaction reconstituted *in vitro* with purified yeast proteins. As a substrate for helicase loading we used linear DNA containing the ARS1 origin sequence. This sequence features a high affinity ORC binding site (ACS), mapping 42 bp upstream of an inverted low affinity site (B2; Fig. 1a)[5,20]. Given that DHs passively slide on duplex DNA[1,6,7,21], we were unable to retain MCM particles on ARS1-DNA tethered to streptavidin-coated magnetic beads. We reasoned that nucleosomes, which naturally flank ARS1 *in vivo*[22], might function as roadblocks to limit DH sliding (Fig. 1b). Indeed, nucleosome-capped ARS1, but not naked ARS1, retains loaded MCM after high-salt wash. The same result is obtained by chromatinizing naturally occurring ARS1 flanking sequences (Extended Data Fig. 1a) or strong-positioning Widom sequences that are biochemically more tractable (Fig. 1c).

Bead-free helicase loading reactions analysed by EM show efficient DH formation as well as class averages containing isolated MCM-Cdt1, ORC, nucleosome or nucleosome close to ORC (Fig. 1d and Extended Data Fig. 1b). To establish whether efficient DH formation requires a specific ORC-nucleosome interaction, we repeated the MCM loading reaction replacing nucleosome caps with M.HpaII methyltransferase (MH) adducts (Extended Data Fig. 1c). We find that MCM loading efficiency is unperturbed, indicating that nucleosomes in our assay primarily serve as roadblocks that prevent DH sliding. To discriminate between

ORC binding at ACS vs B2, we designed new asymmetric substrates containing either a nucleosome upstream of ACS and an MH 75 bp downstream of the B2 element (nucleosome-MH), or the inverse (MH-nucleosome; Extended Data Fig. 1d). EM imaging of ORC binding revealed virtually identical ORC views, mapping in very close proximity to the nucleosome or MH adduct, depending on which neighbored the ACS (Fig. 1e). This result demonstrates that ORC's preference for the ACS high-affinity site is unaffected by nucleosomes.

As duplex DNA is flexible, single-particle 2D averaging failed to capture the whole context of ORC bound to the ARS1 origin; precluding, for example, the identification of multiple ORC binding events on a single origin. To understand origin architecture during DH formation, we established an *in silico* reconstitution approach ("ReconSil") to generate signal-enhanced views of entire replication origins (Extended Data Fig. 2). To this end, we computationally re-assembled origins by substituting raw particles with class averages, re-oriented using particle coordinates from the original micrographs and alignment parameters from 2D classification. Criteria employed to ensure that particles mapped on the same origin DNA are detailed in the Methods and Extended Data Figure 2. To validate this approach, we measured a set of 226 MH-nucleosome ORC-bound ReconSiled origins and found an average length of 141 bp with a standard deviation of 11 bp. The expected distance between the terminal MH and nucleosome roadblocks is 143 bp.

Our ReconSil experiments show 70% (165/236) of origins bound by a single ORC at the ACS (Fig. 1f), 4% (10/236) bound only at the B2 site and 26% (61/236) simultaneously engaged by two ORCs. The distinctive 2D views of ORC enable assignment of the relative ORC orientations (Fig. 1f). In 18% of cases (43/236, only 70% of doubly-populated origins), two ORCs are oriented with their MCM-interacting domains facing one another, as predicted by a symmetric mechanism for DH formation[5,23] (Fig. 1f).

Next, we performed a helicase recruitment assay using ATPγS to capture OCCM complexes on asymmetric nucleosome-MH origins. Like origins bound by ORC alone, 71% (180/255) of ReconSiled origins are engaged by a single OCCM at the ACS, and only 2% (4/255) by a single OCCM at B2 (Fig. 1g and Extended Data Fig. 2d). The remaining 71 origins were simultaneously bound by either two OCCM or OCCM and ORC, although they rarely (12/255 or 17% of doubly-populated origins) had ORC/OCCM in the inverted orientation predicted for a simple symmetric mechanism of loading (Fig. 1g).

## Time-resolved experiments uncover an unexpected MCM-ORC interaction

To interrogate the mechanism of DH formation, we performed an MCM loading time-course assay in ATP for EM imaging at 2, 6 and 20 minutes after MCM addition. As expected, by quantifying the percentage of particles contributing to MCM-containing classes, we observed a decrease in MCM-Cdt1 complexes (69, 38 and 22%), compensated by an increase in DHs (10, 47 and 67%). A subset of OCCM particles (5%) appeared at 2 minutes, and nearly vanished after 20 minutes (1%; Fig. 2a). Thus, OCCM forms in ATP and disappears as DHs assemble, strongly supporting its role as role as a *bona fide* loading intermediate.

A fourth species peaked at 2 minutes (15% of MCM containing particles; Fig. 2a) and gradually tailed off. This species apparently contains one ORC complex, poised ~90 degrees offset from the central channel of a single MCM ring (Fig. 2a). The composition and architecture of this species suggested it may be a loading intermediate, formed downstream of OCCM, perhaps involved in second MCM hexamer recruitment. We reasoned that its continued presence throughout the time-course may result from MCM-depletion preventing DH formation. Accordingly, by adjusting MCM concentration and loading time, we were able to enrich for this MCM-ORC species (Extended Data Fig. 3a).

To understand the nature of this novel MCM-ORC interaction, we solved the 4.4 Å resolution cryo-EM structure (Fig. 2b, Extended Data Fig. 3b-g, 4 and Extended Data Table 1). Rigid body fitting of available ORC-DNA[18] and MCM-DNA[6,7,24] structures confirms that this DNA-bound complex contains an MCM hexamer that interacts with ORC (Fig. 2b).

In our structure, MCM and ORC are connected by two elements. The first is duplex DNA that becomes bent as it runs through the ORC cavity; it remains solvent exposed as it occupies a gap in the protein structure and traverses the entire MCM channel (Fig. 2b). A cut-through view reveals DNA density spanning 88 bp (Fig. 2b). A second element tethering ORC to MCM involves C-terminal Orc6 and a previously unresolved protein module. Given its position, we postulated that this element could be the N-terminal domain of Orc6, which has so far eluded structural characterization. In agreement with published bioinformatics analysis[19], our homology modelling of N-terminal yeast Orc6, reveals a TFiiB like fold (discussed in Extended Data Figure 5). Docking of the new N-terminal Orc6 model into the cryo-EM map resulted in an excellent fit (Fig. 2c). Combining this new structural information with the ORC and MCM structures, we refined a near-complete atomic model of the full DNA-bound complex (Supplementary Video 1), which we named **M**CM-**O**RC (**MO**).

Two aspects of the structure deserve attention. First, MO lacks Cdc6 and Cdt1 (Fig. 3 and Extended Data Fig. 6). ATP hydrolysis is known to promote Cdt1 ejection and MCM ring closure[4,11,13,15]. Coherently, we find that the Mcm2-5 gate in MO is closed, whilst the nucleotide occupancy of MCM matches that of a loaded (post-catalytic) DH, with empty MCM sites 4-6 and 7-4 and nucleotide-bound 6-2, 2-5, 5-3 and 3-7 (likely ADP, Fig. 3a)[7]. Moreover, molecular docking reveals that MCM in MO is virtually identical to an MCM hexamer in the DH[6,7] (Supplementary Video 2). Thus, MO contains a single-loaded helicase ring, supporting our hypothesis that MO occurs after the OCCM intermediate[15].

Second, ORC in MO binds DNA in an inverted configuration with respect to the upstream ACS element, and interacts with the N- and not the C-terminal side of the MCM ring, in contrast to ORC in OCCM[17] (Fig. 3b-d). This mode of binding requires MCM gate closure, so that the Orc6 N- and C-terminal elements can latch across Mcm2 and Mcm5 (the DNA gate subunits, Fig. 2b and Extended Data Fig. 5d, e). In doing so, Orc6 also engages a protein surface involved in MCM homo-dimerisation in a DH[16] (Fig. 3).

## N-terminal Orc6 promotes efficient DH formation

To investigate whether the MCM-ORC interaction observed in MO has a role in double-hexamer formation, we sought to impair the Orc6/Mcm2-5 interface. Orc1-5 can recruit MCM to origins in ATPγS but releases MCM from DNA in ATP[4,25]. We therefore performed a subtler Orc6 truncation that lacks the N-terminal domain (precluding Mcm2 engagement) but retains the Cdt1 interaction essential for MCM loading[9,25,26]. To this end, we generated an ORC variant, lacking the N-terminal 119 amino acids of Orc6 (hereafter, Δ119). Using a bead-based pull-down assay we show that Δ119 recruits MCM in ATPγS to wild type levels (Fig. 4a) and efficiently forms OCCM as shown by EM analysis (Fig. 4b). However, ATP-promoted MO formation decreased by ~50% compared to wild type ORC. Notably, Δ119 MOs have an altered ORC conformation (Supplementary Video 3). Thus, removing just one component of the MCM-ORC interaction interface negatively affects MO formation (Fig. 4c).

Coherent with the notion that MO is a *bona fide* loading intermediate, when ORC is replaced by Δ119 *(i)* DH retention on DNA beads drops in an *in vitro* helicase loading reaction subjected to low or high-salt washes (Fig. 4a); (*ii*) DH counts decrease by 2.6-fold in the MO formation EM assay (Fig. 4c); (*iii*) DH formation is significantly slowed in a negative stain EM time-course experiment (Fig. 4d). The impaired ability of Δ119 to load DHs may explain a previous observation that an Orc6 lacking amino acids 1-73 cannot complement an Orc6 deletion *in vivo*[9].

## A sequential mechanism for head-to-head MCM double hexamer formation

We used time-resolved EM to show that OCCM is a *bona fide* reaction intermediate forming at ACS sites, on path to loading the first MCM hexamer. To further understand first-hexamer recruitment we performed an analogous cryo-EM experiment using an early time point and conditions optimised to capture a pre-OCCM state. Aside from reproducing the expected ATP-OCCM in vitreous ice, we also identified a 2D class where ORC-Cdc6 is yet to fully engage MCM-Cdt1 to form OCCM (hereafter, OC-MC; Fig. 5a and Extended Data Fig. 7a, b). Here, duplex DNA is poised for threading into the MCM channel, being bent by ORC and aligned with the Mcm2-5 gate. We confirm this observation by comparing ReconSiled origins containing OC-MC and OCCM particles obtained in our DH formation time course experiment (Extended Data Fig. 7c, d) This finding reveals an initial helicase-engagement mode on path to first MCM loading.

As ORC in MO recognizes a closed MCM ring at the MCM dimerization interface, we postulated that this state might reflect a downstream ORC binding event, on path to second ring recruitment. Indeed, MO and OCCM structure superposition reveals that ORC-induced DNA-bending in MO creates sufficient space for the inverted ORC to accept a second MCM ring via the same interactions that forms OCCM[4] (Extended Data Fig. 8a, b). In this model, the Mcm2-5 gate in the second incoming MCM would align to the solvent-exposed bent DNA in MO, and therefore be perfectly positioned for DNA threading into the MCM channel.

In negative-stain EM experiments, we successfully captured this predicted state by supplementing MO with MCM-Cdt1 to visualise second MCM hexamer engagement (Extended Data Fig. 8c). In a parallel effort, sub-classification of MO images in the cryo-EM dataset allowed us to identify the same second-ring recruitment species (Fig. 5a and Extended Data Fig. 8d). Clear DNA visualization possible with cryo-EM reveals that this species contains DNA bent and aligned with the Mcm2-5 gate, virtually identical to the OC-MC described above (Fig. 5a, Extended Data Fig. 8d, e and Supplementary Video 4).

Single-molecule studies showed that first and second MCM loading require distinct Cdc6 molecules[15]. To investigate if MO-dependent DH formation requires Cdc6, we formed MO and immunodepleted Cdc6, before supplementing MOs with MCM-Cdt1. Strikingly, MOs could not load DHs in the absence of additional Cdc6 (Extended Data Fig. 8f). Therefore, we confirm that first and second MCM ring loading occur via the same Cdc6-dependent OC-MC mechanism.

In summary, time-resolved EM analysis of MCM loading, using wild type proteins and ATP, have allowed us to identify intermediates on path to DH formation. First ORC and then Cdc6 bind to high-affinity ACS sites and recruit a first MCM via an interaction between the ORC and MCM C-terminal domains. During this process, bent DNA is threaded through the MCM channel, forming OCCM. After Cdc6/Cdt1 release and MCM ring closure, an inverted ORC engages the MCM N-terminal homo-dimerisation interface, forming MO. Second ORC engagement can occur before first ORC release is complete, as shown by an intermediate containing a loaded MCM flanked by two ORCs (named $O_2M$; Extended Data Fig. 9). Once engaged, N-terminal ORC recruits a second Cdc6 and MCM-Cdt1, forming an MOC-MC intermediate. As with first ring loading, ORC is poised for threading the bent DNA through the Mcm2-5 gate, eventually resulting in DH formation[1,2]. Our 2D averages can be used as frames to generate a movie of the entire DH formation reaction, which closely matches a molecular morph movie generated by interpolating between atomic models of distinct loading intermediates (Fig. 5a-c and Supplementary Video 4).

Recruitment of a second ORC to origin DNA has been shown to require a secondary inverted ORC binding site; however, its precise sequence and distance from ACS varies between origins[5,20,27,28]. Therefore, DH formation might require sliding of MCM loading intermediates[5,27].

Using ReconSil we show that, similar to DHs, single MCMs can slide on origin DNA[1,6,7]. In fact, MCMs from both MO and MOC-MC intermediates are often found adjacent to the nucleosome, occupying the ACS site originally engaged by the first ORC (Fig. 5d and Extended Data Fig. 9). In the MO intermediate, 66 bp of DNA span the DNA entry point into MCM and the ORC-engagement site. 66 bp is also the distance separating the nucleosome positioning sequence and B2 in our construct. Therefore, loaded MCM sliding allows inverted ORC engagement at B2, which would otherwise be sterically occluded by the first loaded hexamer on an ARS1 origin. In this context, ORC could simultaneously engage MCM and B2, increasing its specificity and affinity for the B2 site. This could explain why ORC engagement downstream of the ACS can occur in either orientation when imaged in ORC-binding or MCM-recruitment ATPγS assays (Fig. 1f, g), while inverted

ORC occupancy is assured in the presence of a single loaded MCM. Thus, MO formation ensures that second ORC association occurs with the correct orientation for head-to-head DH formation. This model has important implications for helicase loading mechanism in higher eukaryotes, as discussed in the Supplementary Information.

Our data explain how DH loading onto replication origins is symmetrical (two inverted ORC assemblies recruit two MCM rings via the same OCCM mechanism[4,5]) as well as sequential/coordinated (loading of the first MCM ring drives loading of the second ring[3]). Therefore, our model reconciles two apparently contrasting studies on the mechanism of DH formation.

## Extended Data



Europe PMC Funders Author Manuscripts

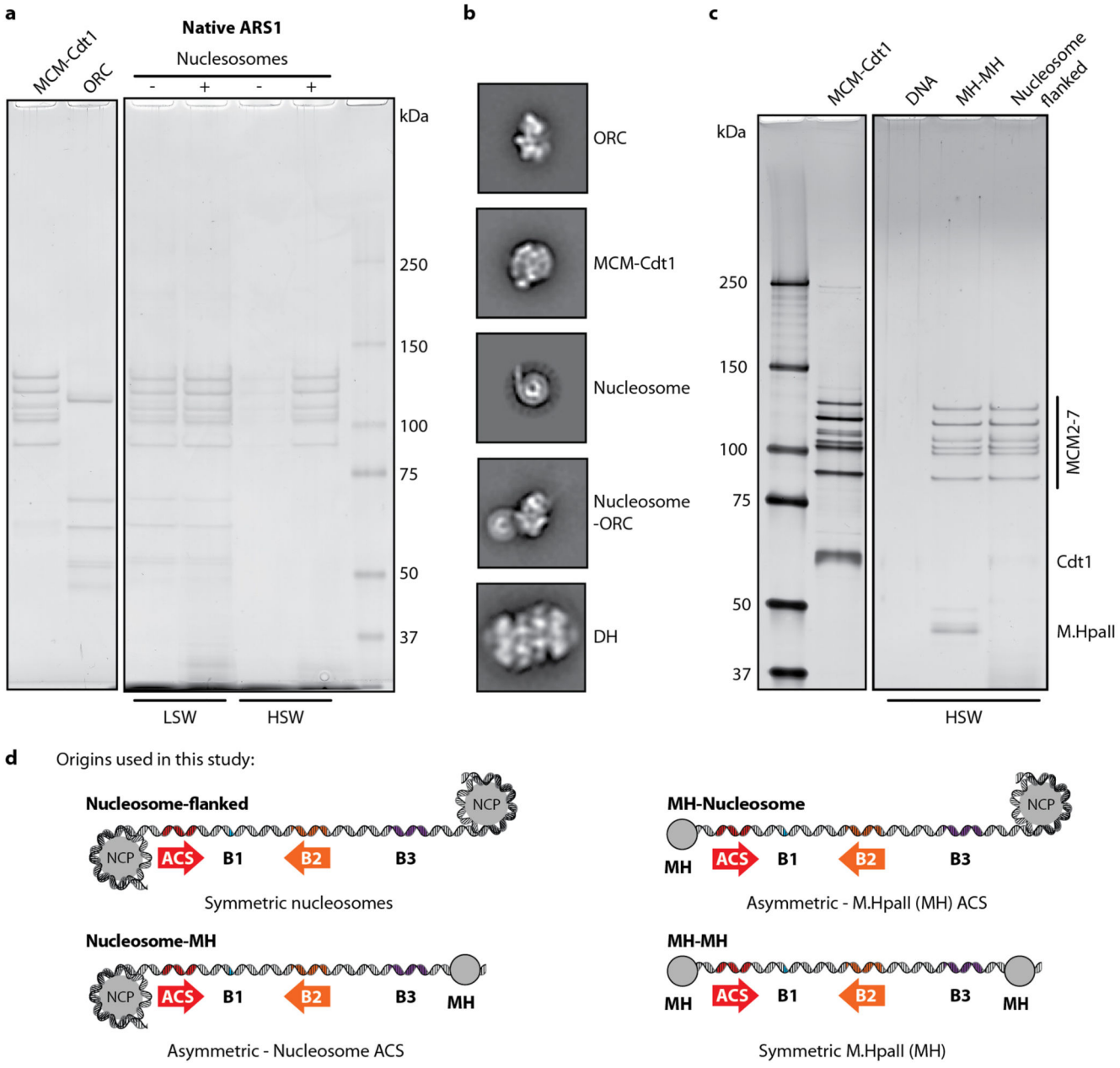


**Extended Data Figure 1.**

Nucleosomes function as roadblocks that limit the linear diffusion of DHs. **(a)** While loaded MCM particles are retained on short naked DNA when washed with low salt (300 mM NaOAc, LSW), they slide off DNA when washed with high salt (500 mM NaCl, HSW). When chromatinised, the same DNA substrate retains MCM particles. In this experiment, soluble MCM loading reactions are bound to streptavidin-coated magnetic beads via a desthiobiotin tag on the origin DNA, prior to removing unbound proteins with high or low salt washes. **(b)** EM imaging of soluble MCM loading reactions yields 2D class averages of licensing complexes on chromatinised DNA. Despite the sample heterogeneity, recognizable classes can be obtained for ORC, MCM-Cdt1, nucleosomes and ORC mapping in close




Europe PMC Funders Author Manuscripts

proximity to a nucleosome, as well as DHs. **(c)** Comparison between MCM loading on chromatinised DNA and DNA containing MH roadblocks. After HSW treatment, equal amounts of loaded MCMs are retained on streptavidin beads, indicating that nucleosomes are not required for efficient DH formation in this assay. **(d)** Yeast replication origins centered on ARS1, containing two inverted ORC binding sites named ACS (ARS consensus sequence) (high affinity, red arrow) and B2 (low affinity, orange arrow). ARS1 is flanked by nucleosomes, covalently attached methyltransferases (MH-MH), or a combination of the two to obtain asymmetric origins with recognizable features marking the ends of the origin (MH-nucleosome and nucleosome-MH). For gel source data for (a) and (c), see Supplementary Fig. 1

Europe PMC Funders Author Manuscripts

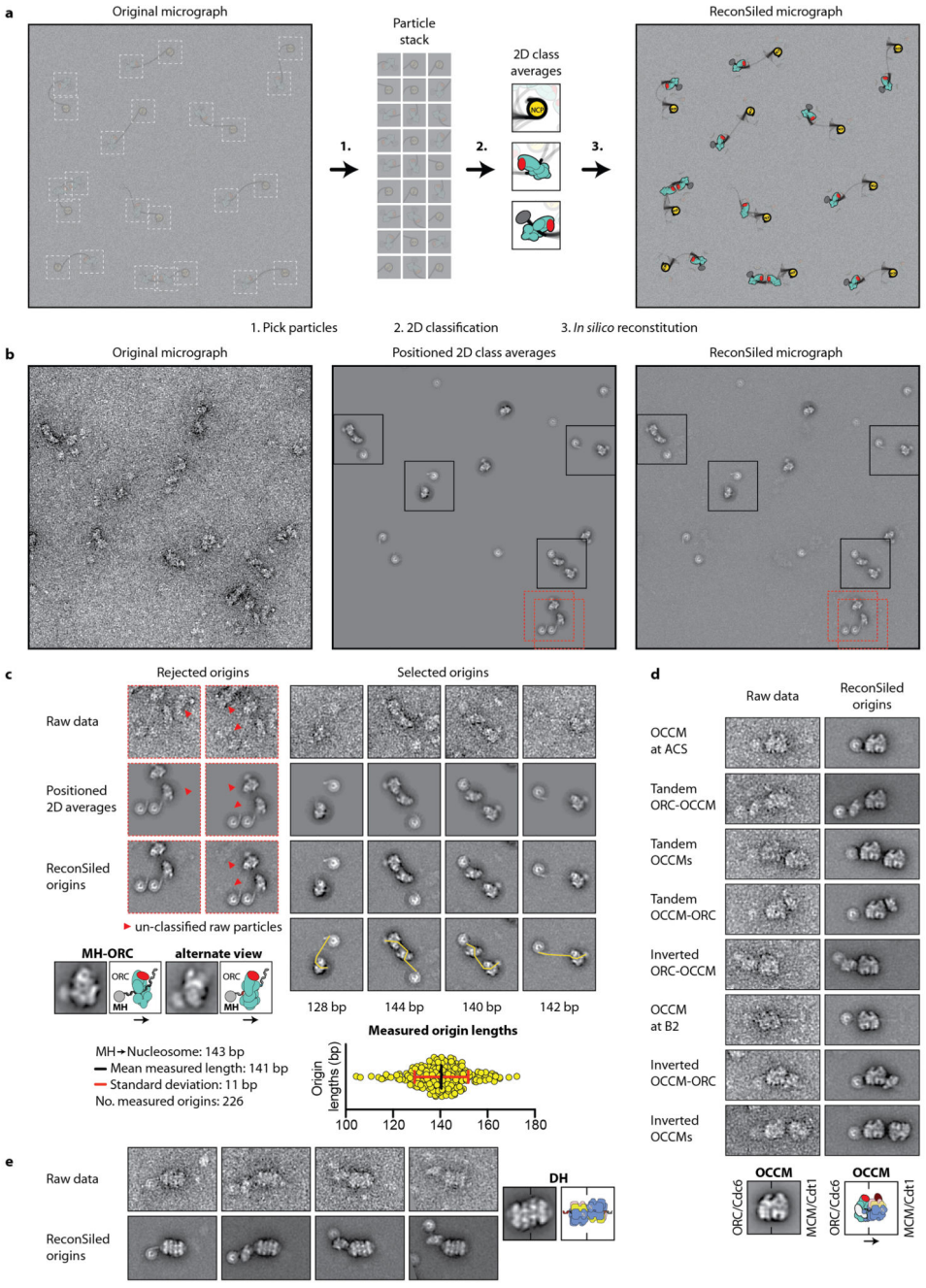


**Extended Data Figure 2.**

*In silico* reconstitution (ReconSil) of origin licensing performed on asymmetric origins of replication. **(a)** Cartoon representation depicting the ReconSil procedure as performed to investigate the interactions between ORC and an asymmetric origin. Particles are picked on micrographs with a low signal-to-noise ratio. 2D averages are calculated. Averages are superposed to the raw micrographs, overlaid to the particles that contributed to their generation. For this purpose, particle coordinates are combined with alignment parameters derived from 2D alignment and classification. This approach yields a signal-enhanced view

Europe PMC Funders Author Manuscripts

of single instances of molecular complexes bound to a flexible substrate, in this case, ORC binding to an entire origin of replication. **(b)** Representative raw micrograph, 2D class averages positioned according to their constituent particles, and a ReconSiled micrograph with positioned 2D class averages overlaid onto the original image. Instances boxed in black are selected, red are rejected. **(c)** Left, origins might be rejected due to local particle clustering/aggregation or because they contain visible raw particles that could not be aligned and classified and therefore, are not matched by a high-quality 2D average. This assay utitlised MH-nucleosome origins that permit measurement of the length of ReconSiled origins because both the MH roadblock (next to ACS-bound ORC) and the nucleosome can be reconstituted. Measurement of ReconSiled origins was performed using ImageJ. **(d)** Comparison of raw NS data and ReconSiled origins for representative OCCM-bound origins shown in Figure 1g. **(e)** Example ReconSiled origins (and corresponding raw data) showing DHs recruited to nucleosome-MH origins. ORC frequently rebinds to the ACS on origins containing DHs, but shows no fixed interaction with the C-terminal face of loaded DH.

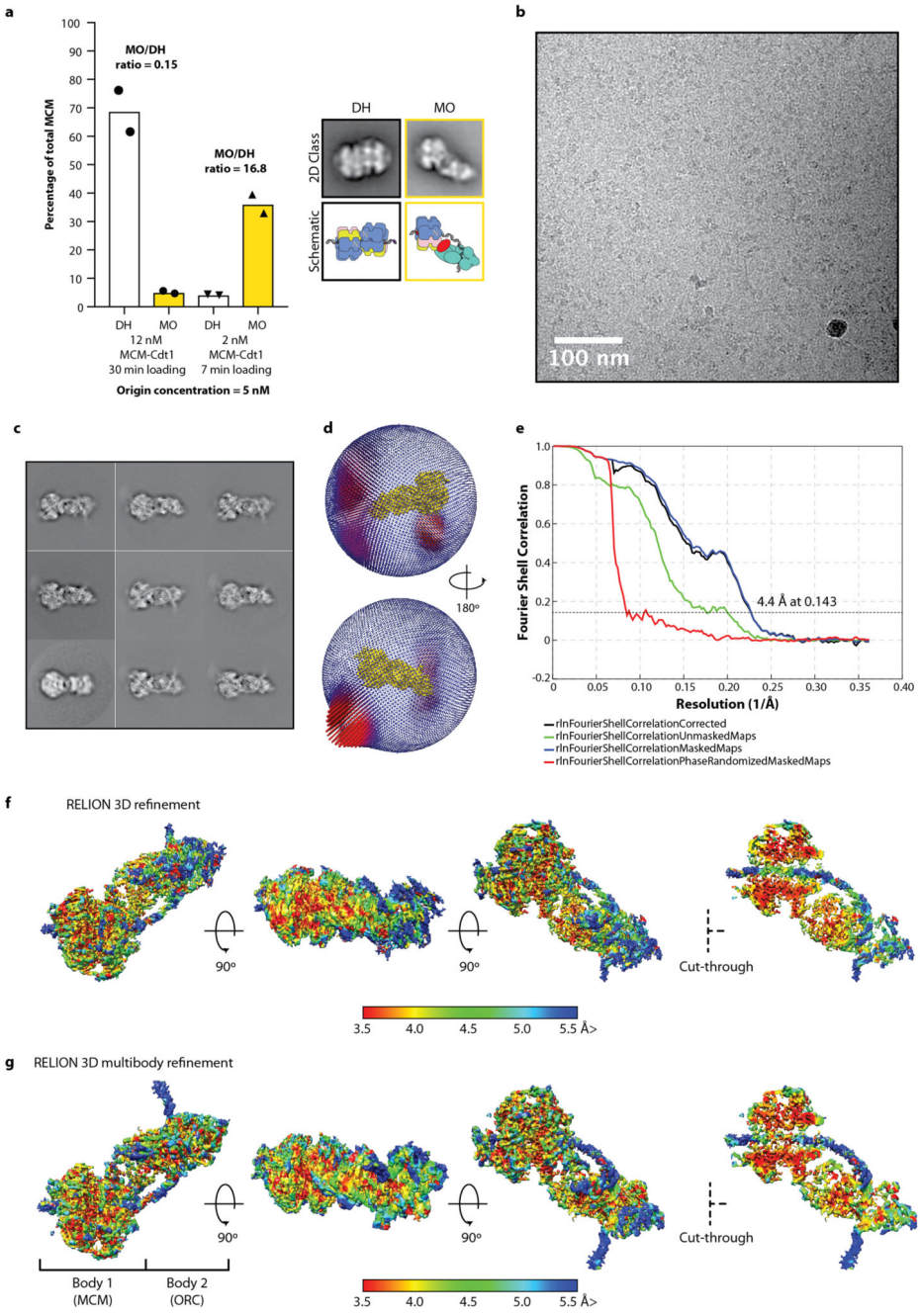


**Extended Data Figure 3.**

Cryo-EM structure of the MCM-ORC loading intermediate (MO). **(a)** The MO intermediate is enriched when MCM-Cdt1 concentration is limiting, as quantified using negative stain EM. An MCM loading reaction performed for 30 minutes in the presence of excess MCM-Cdt1 results in the majority of MCMs forming DHs on DNA. If MCM-Cdt1 concentration is limited and loading time is reduced (7 minutes), MO complexes form but do not mature into DHs, indicating that the MO intermediate is on-path to DH formation. Bar chart shows mean, n=2 independent experiments. **(b)** Example of an aligned movie. **(c)** Resulting 2D

averages. **(d)** Angular distribution. **(e)** Resolution estimated using gold-standard Fourier Shell Correlation. **(f)** Three rotated views and a cut-through view of the MO 3D structure, color-coded according to local resolution. **(g)** Structure obtained by multi-body refinement, displayed as described for panel e.



Europe PMC Funders Author Manuscripts

Europe PMC Funders Author Manuscripts

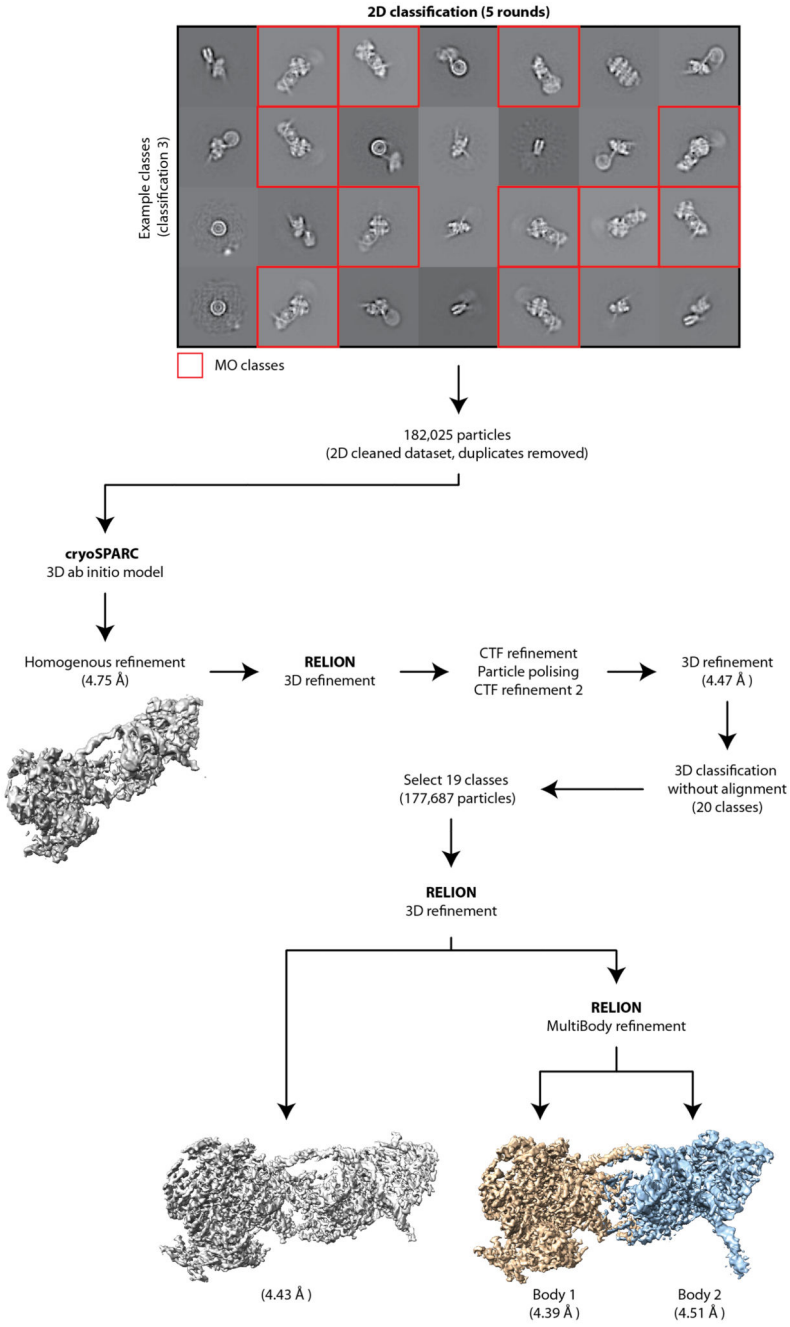


**Extended Data Figure 4.**
Classification and refinement pipeline for the MO structure.

Europe PMC Funders Author Manuscripts

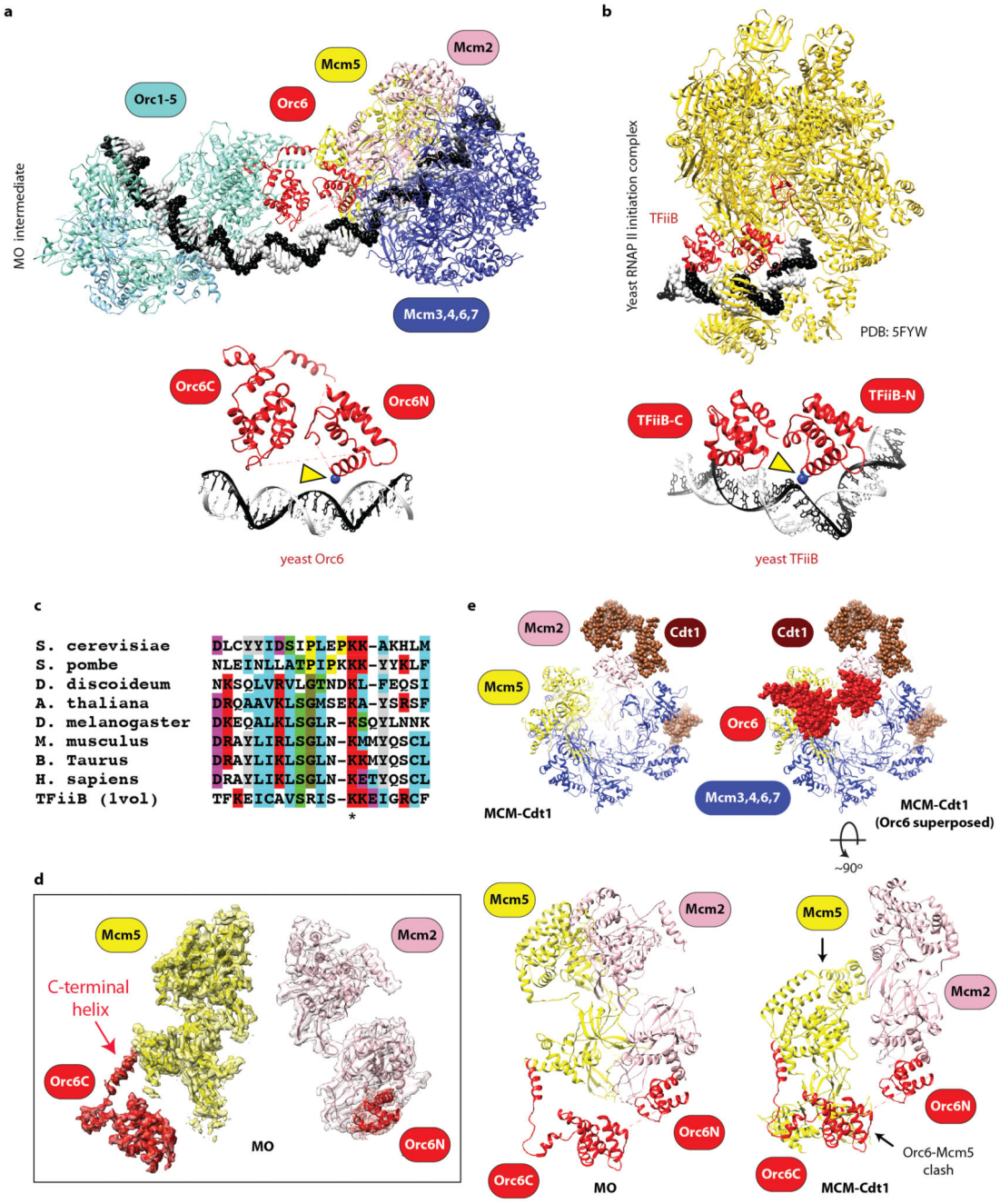


**Extended Data Figure 5.**

A role for Orc6 in modulating MCM loading. **(a)** Two elements connect ORC and N-terminal MCM. One is Orc6, the second is DNA, which is solvent exposed between the ORC and MCM complexes due to the bend induced by complex formation. **(b)** Orc6 contains a domain architecture preserved in the related TFiiB transcription factor[46]. Although the precise mode of DNA engagement for the N- and C-terminal domains of TFiiB and Orc6 differ, notable conservation can be detected. **(c)** Sequence alignment between N-terminal TFiiB and N-terminal Orc6. The N-terminal domain of Orc6 contacts DNA through

a conserved lysine also found in TFiiB. Mutation of the equivalent lysine in *Drosophila* Orc6 affects DNA binding *in vitro* and replication in extracts and cells[47]. **(d)** A conserved helix[18],[48] of the Orc6 C-terminal domain (Orc6C) touches the N-terminal helical bundle of Mcm5. Orc6 N-terminal domain (Orc6N) touches the N-terminal helical bundle of Mcm2. Together the NTD and CTD of Orc6 latch across the Mcm2-5 gate. **(e)** No steric clash can be detected between Orc6 and Cdt1 when MO and MCM-Cdt1 are superposed via N-terminal Mcm2. However, C-terminal Orc6 severely clashes with N-terminal Mcm5 in this configuration. Only Orc6 from MO is shown in the MCM-Cdt1 superposed structure.

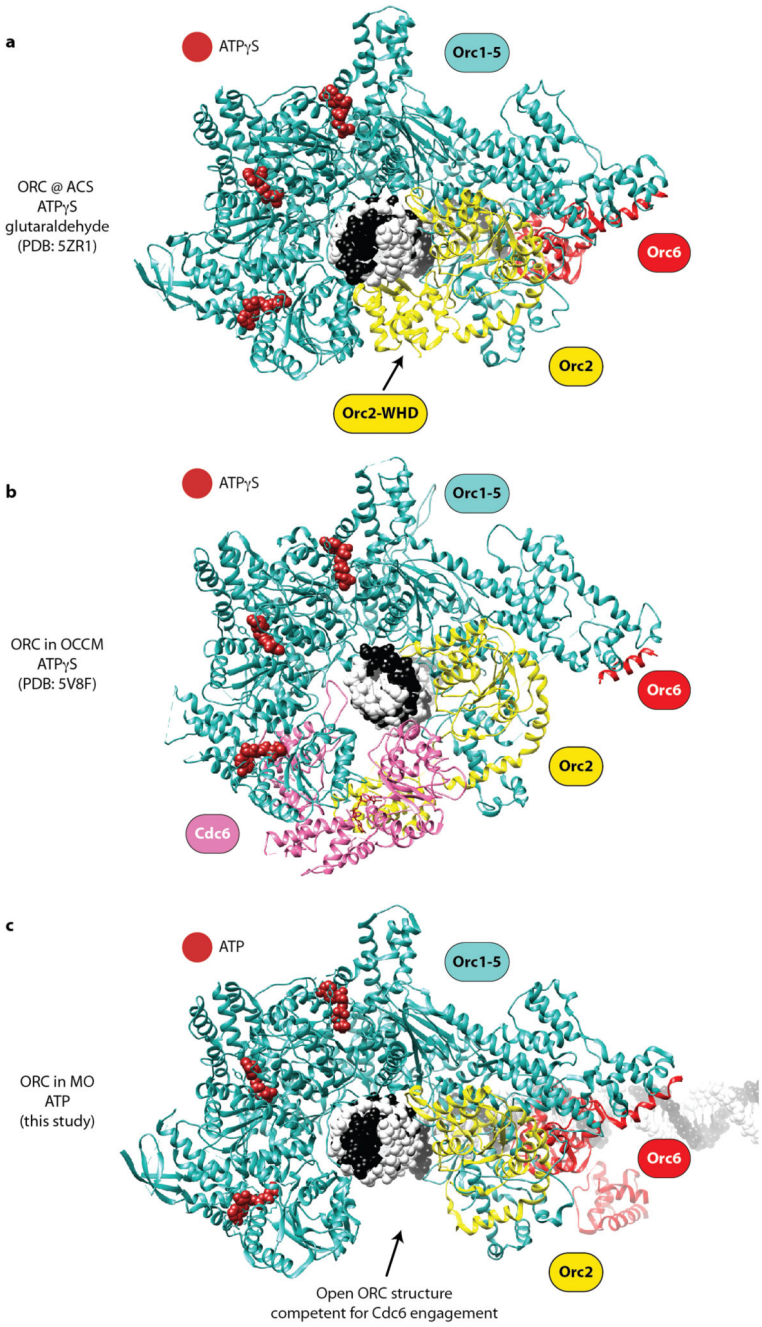


**Extended Data Figure 6.**

Structure of ORC-DNA in different states. Comparison between the cross-linked ORC-DNA complex imaged in isolation **(a)**, ORC-DNA in the OCCM complex **(b)** and ORC-DNA in the MO complex **(c)**. Nucleotide occupancy appears the same. It should be noted however that ORC-DNA alone and within the OCCM complex were co-incubated with ATPγS, while ORC in MO was imaged in ATP. Orc2 in ORC-DNA contains a visible winged-helix domain (WHD) topologically closing ORC around DNA. ORC in OCCM is Cdc6 engaged. Cryo-EM density for the Orc2 WHD domain is virtually absent in the MO complex, indicating

that this domain is flexible. This difference might reflect a different ORC configuration in MO, or the fact that the previously published ORC-DNA structure was stabilized by glutaraldehyde crosslinking. Despite Cdc6 being present in the sample, ORC in MO is not Cdc6 bound.



Europe PMC Funders Author Manuscripts

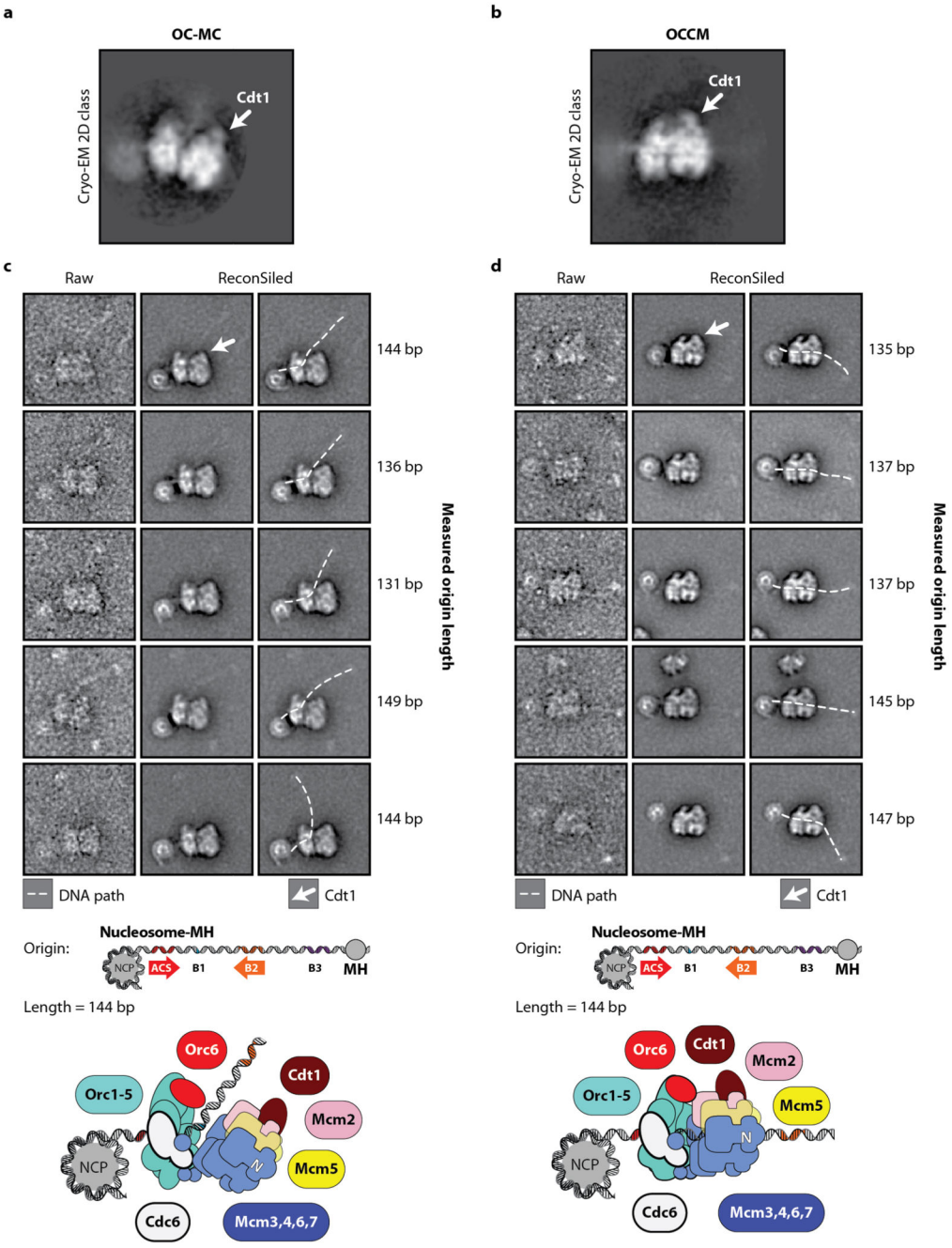


**Extended Data Figure 7.**

OC-MC contains a recruited, but not DNA-engaged MCM-Cdt1. **(a,b)** Cryo-EM 2D class averages indicate that OC-MC is a pre-OCCM intermediate. This finding is confirmed by comparison of raw and ReconSiled origins, which permit visualization of the DNA path through OC-MC **(c)** and OCCM **(d)** in negative stain experiments. In OC-MC, MCM-Cdt1 has engaged a DNA bound ORC complex, however, DNA remains outside the MCM channel. In this configuration, DNA is aligned to the Mcm2-5 gate, which can be located in the 2D images because of its proximity to the prominent N-terminal lobe of Cdt1 (white

arrow). In contrast, DNA runs through the central channels of both ORC and MCM in the OCCM complex, in preparation for Cdt1 release and MCM ring closure.



Europe PMC Funders Author Manuscripts

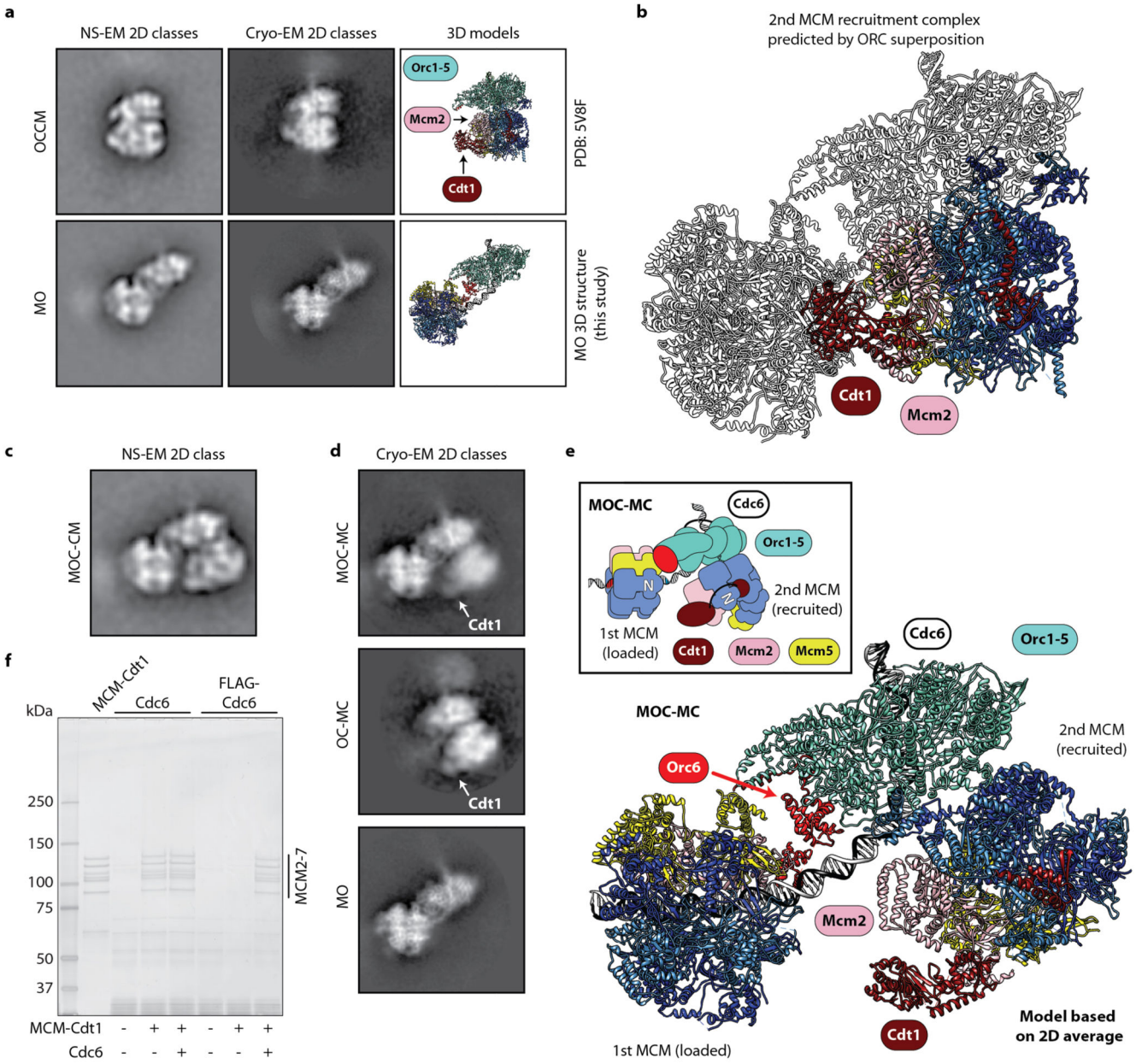


**Extended Data Figure 8.**

ORC in MO is perfectly positioned for loading the second MCM ring in the correct orientation for DH formation. **(a)** Negative stain and cryo-EM 2D classes, and 3D structures of OCCM (top row) and MO (bottom row), with the loading intermediates aligned via their respective ORC complexes. **(b)** 3D model based on panel (a) of the proposed mechanism for second MCM recruitment. OCCM is shown superposed to MO's ORC. This superposition places a second MCM-Cdt1 so that its Mcm2-5 gate is oriented for threading duplex DNA into the MCM channel. **(c)** Negative stain 2D class showing a post-MO loading intermediate, captured by supplementing MO complexes with MCM-Cdt1 prior to imaging. This class appears to be a second MCM recruitment complex, containing MO and an




Europe PMC Funders Author Manuscripts

additional MCM-Cdt1. **(d)** A cryo-EM 2D class average of the post-MO complex (top panel) shows bent duplex DNA aligned to the Mcm2-5 DNA gate of the second MCM-Cdt1, captured before DNA threading. This is the same configuration previously identified for the OC-MC complex (second panel). Alignment of the OC-MC and MO 2D classes by their respective ORCs shows that the second MCM recruitment complex contains a loaded MCM ring and OC-MC, connected via the DNA and Orc6; we named this complex MOC-MC. **(e)** 3D model of MOC-MC, based on MO structure and 2D class averages shown in (c) and (d). **(f)** Cdc6 is required for loading of the second MCM helicase. Following immunodepletion of FLAG-tagged Cdc6, MO is unable to load a second MCM resulting in a failure to form salt-stable DHs on DNA in the absence of additional Cdc6. For gel source data, see Supplementary Fig. 1.

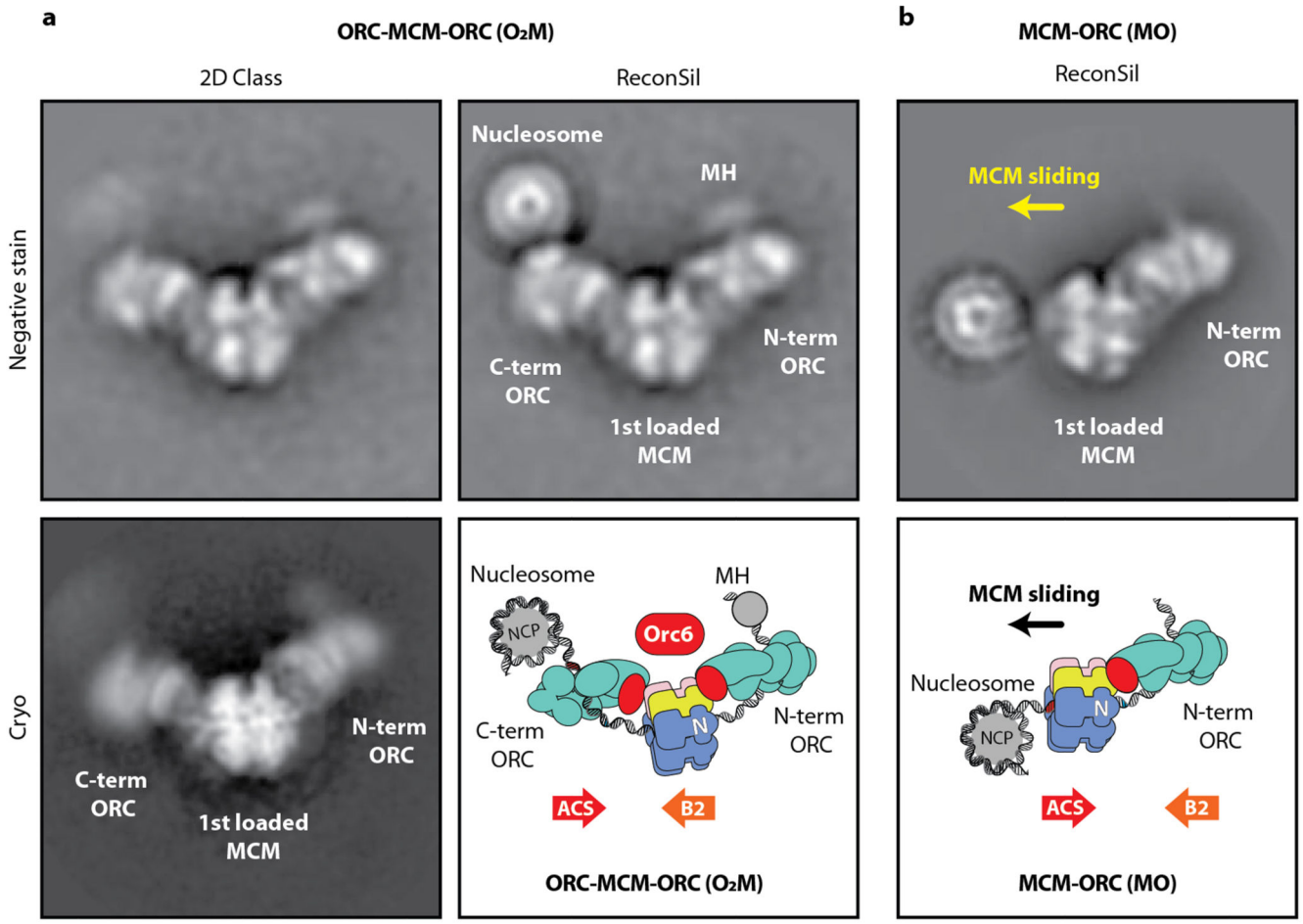


**Extended Data Figure 9.**

A second ORC can bind to a loaded MCM helicase prior to first ORC release. **(a)** Negative stain 2D class, ReconSiled nucleosome-MH origin, cryo EM 2D class and schematic showing a DH formation intermediate containing a single loaded MCM helicase (Cdt1 has been released) flanked by ORC at its C and N termini ($O_2M$). ReconSiled origin shows an entire origin spanning nucleosome, C-terminal ORC, MCM hexamer, N-terminal ORC and covalently linked M.HpaII (MH) **(b)** ReconSiled nucleosome-MH origin bound by MO and associated schematic. MO was imaged with MCM occupying the ACS site, which must previously have been occupied by an ORC (as seen in the $O_2M$ complex in (a)), demonstrating that MCM sliding towards the nucleosome has occurred.

**Extended Data Table 1**

**Cryo-EM data collection, refinement and validation statistics.**

| | MO (EMDB-4980) (PDB 6RQC) |
|---|---|
| **Data collection and processing** | |

Europe PMC Funders Author Manuscripts

| | MO (EMDB-4980) (PDB 6RQC) | |
|---|---|---|
| Magnification | 105,000 | |
| Voltage (kV) | 300 | |
| Electron exposure (e–/Å$^2$) | 50.4 | |
| Defocus range (μm) | -2.7 to -4.2 | |
| Pixel size (Å) | 1.38 | |
| Symmetry imposed | C1 | |
| Initial particle images (no.) | 6,287,507 | |
| Final particle images (no.) | 177,687 | |
| Map resolution (Å) | 4.4 | |
| FSC threshold | 0.143 | |
| Map resolution range (Å) | 3.3 – 6.3 | |
| **Refinement** | | **Model Resolution** |
| Initial model used (PDB code) | 5ZR1 (ORC-DNA) | 3.0 |
| | 6EYC (MCM-DH) | 3.8 |
| | 6F0L (MCM-DH-DNA) | 4.8 |
| | 5BK4 (MCM-DH-DNA) | 3.9 |
| FSC threshold | 0.143 | |
| Map sharpening ***B*** factor (Å$^2$) | -149.415 | |
| Model composition | | |
| Non-hydrogen atoms | 53,245 | |
| Protein and DNA residues | 6350 | |
| Ligands (ATP, ADP, $Mg^{2=}$, $Zn^{2+}$) | 15 | |
| ***B*** factors (Å$^2$) | | |
| Protein | 129.87 | |
| Nucleotide | 267.34 | |
| Ligand | 128.76 | |
| R.m.s. deviations | | |
| Bond lengths (Å) | 0.009 | |
| Bond angles (°) | 1.411 | |
| Validation | | |
| MolProbity score | 2.04 | |
| Clashscore | 8.98 | |
| Poor rotamers (%) | 0.54 | |
| Ramachandran plot | | |
| Favored (%) | 89.5 | |
| Allowed (%) | 10.4 | |
| Disallowed (%) | 0.1 | |

## Supplementary Material

Refer to Web version on PubMed Central for supplementary material.

## Acknowledgements

The authors would like to thank past and present members of the Costa lab for useful discussions and Gideon Coster, Allison McClure, Christoph Kurat, Anne Early and Lucy Drury for sharing reagents/purification protocols. A special thanks goes to Stephanie Webb and Noah Turner for help with biochemical and EM experiments. Andrea Nans (Crick Structural Biology STP) for support on the Titan Krios and Raffa Carzaniga (Crick EM STP) for support on the Tecnai G2 Spirit electron microscope. Thanks to Andrew Purkiss and Phil Walker for computational support, and Namita Patel, Alireza Alidoust and Damini Patel for yeast fermentation (Crick Fermentation STP). This work was funded jointly by the Wellcome Trust, MRC and CRUK at the Francis Crick Institute (FC0010065, FC0010066). A.C. receives funding from the European Research Council (ERC) under the European Union's Horizon 2020 research and innovation programme (grant agreement No 820102).

## References

1. Remus D, et al. Concerted loading of Mcm2-7 double hexamers around DNA during DNA replication origin licensing. Cell. 2009; 139:719–730. DOI: 10.1016/j.cell.2009.10.015 [PubMed: 19896182]
2. Evrin C, et al. A double-hexameric MCM2-7 complex is loaded onto origin DNA during licensing of eukaryotic DNA replication. Proc Natl Acad Sci U S A. 2009; 106:20240–20245. DOI: 10.1073/pnas.0911500106 [PubMed: 19910535]
3. Ticau S, Friedman LJ, Ivica NA, Gelles J, Bell SP. Single-molecule studies of origin licensing reveal mechanisms ensuring bidirectional helicase loading. Cell. 2015; 161:513–525. DOI: 10.1016/j.cell.2015.03.012 [PubMed: 25892223]
4. Frigola J, Remus D, Mehanna A, Diffley JF. ATPase-dependent quality control of DNA replication origin licensing. Nature. 2013; 495:339–343. DOI: 10.1038/nature11920 [PubMed: 23474987]
5. Coster G, Diffley JFX. Bidirectional eukaryotic DNA replication is established by quasi-symmetrical helicase loading. Science. 2017; 357:314–318. DOI: 10.1126/science.aan0063 [PubMed: 28729513]
6. Abid Ali F, et al. Cryo-EM structure of a licensed DNA replication origin. Nature communications. 2017; 8doi: 10.1038/s41467-017-02389-0
7. Noguchi Y, et al. Cryo-EM structure of Mcm2-7 double hexamer on DNA suggests a lagging-strand DNA extrusion model. Proc Natl Acad Sci U S A. 2017; 114:E9529–E9538. DOI: 10.1073/pnas.1712537114 [PubMed: 29078375]
8. Nguyen VQ, Co C, Li JJ. Cyclin-dependent kinases prevent DNA re-replication through multiple mechanisms. Nature. 2001; 411:1068–1073. DOI: 10.1038/35082600 [PubMed: 11429609]
9. Chen S, Bell SP. CDK prevents Mcm2-7 helicase loading by inhibiting Cdt1 interaction with Orc6. Genes Dev. 2011; 25:363–372. DOI: 10.1101/gad.2011511 [PubMed: 21289063]
10. Zhai Y, et al. Open-ringed structure of the Cdt1-Mcm2-7 complex as a precursor of the MCM double hexamer. Nature structural & molecular biology. 2017; 24:300–308. DOI: 10.1038/nsmb.3374
11. Frigola J, et al. Cdt1 stabilizes an open MCM ring for helicase loading. Nature communications. 2017; 8doi: 10.1038/ncomms15720
12. Coster G, Frigola J, Beuron F, Morris EP, Diffley JF. Origin licensing requires ATP binding and hydrolysis by the MCM replicative helicase. Mol Cell. 2014; 55:666–677. DOI: 10.1016/j.molcel.2014.06.034 [PubMed: 25087873]
13. Kang S, Warner MD, Bell SP. Multiple functions for Mcm2-7 ATPase motifs during replication initiation. Mol Cell. 2014; 55:655–665. DOI: 10.1016/j.molcel.2014.06.033 [PubMed: 25087876]
14. Fernandez-Cid A, et al. An ORC/Cdc6/MCM2-7 complex is formed in a multistep reaction to serve as a platform for MCM double-hexamer assembly. Mol Cell. 2013; 50:577–588. DOI: 10.1016/j.molcel.2013.03.026 [PubMed: 23603117]
15. Ticau S, et al. Mechanism and timing of Mcm2-7 ring closure during DNA replication origin licensing. Nature structural & molecular biology. 2017; 24:309–315. DOI: 10.1038/nsmb.3375
16. Li N, et al. Structure of the eukaryotic MCM complex at 3.8 A. Nature. 2015; 524:186–191. DOI: 10.1038/nature14685 [PubMed: 26222030]

17. Yuan Z, et al. Structural basis of Mcm2-7 replicative helicase loading by ORC-Cdc6 and Cdt1. Nature structural & molecular biology. 2017; 24:316–324. DOI: 10.1038/nsmb.3372

18. Li N, et al. Structure of the origin recognition complex bound to DNA replication origin. Nature. 2018; 559:217–222. DOI: 10.1038/s41586-018-0293-x [PubMed: 29973722]

19. Bleichert F, Leitner A, Aebersold R, Botchan MR, Berger JM. Conformational control and DNA-binding mechanism of the metazoan origin recognition complex. Proc Natl Acad Sci U S A. 2018; 115:E5906–E5915. DOI: 10.1073/pnas.1806315115 [PubMed: 29899147]

20. Palzkill TG, Newlon CS. A yeast replication origin consists of multiple copies of a small conserved sequence. Cell. 1988; 53:441–450. [PubMed: 3284655]

21. Gros J, et al. Post-licensing Specification of Eukaryotic Replication Origins by Facilitated Mcm2-7 Sliding along DNA. Mol Cell. 2015; 60:797–807. DOI: 10.1016/j.molcel.2015.10.022 [PubMed: 26656162]

22. Eaton ML, Galani K, Kang S, Bell SP, MacAlpine DM. Conserved nucleosome positioning defines replication origins. Genes Dev. 2010; 24:748–753. DOI: 10.1101/gad.1913210 [PubMed: 20351051]

23. Robinson NP, Bell SD. Origins of DNA replication in the three domains of life. Febs J. 2005; 272:3757–3766. [PubMed: 16045748]

24. Croll TI. ISOLDE: a physically realistic environment for model building into low-resolution electron-density maps. Acta Crystallogr D Struct Biol. 2018; 74:519–530. DOI: 10.1107/S2059798318002425 [PubMed: 29872003]

25. Chen S, de Vries MA, Bell SP. Orc6 is required for dynamic recruitment of Cdt1 during repeated Mcm2-7 loading. Genes Dev. 2007; 21:2897–2907. DOI: 10.1101/gad.1596807 [PubMed: 18006685]

26. Asano T, Makise M, Takehara M, Mizushima T. Interaction between ORC and Cdt1p of Saccharomyces cerevisiae. FEMS Yeast Res. 2007; 7:1256–1262. DOI: 10.1111/j.1567-1364.2007.00299.x [PubMed: 17825064]

27. Warner MD, Azmi IF, Kang S, Zhao Y, Bell SP. Replication origin-flanking roadblocks reveal origin-licensing dynamics and altered sequence dependence. J Biol Chem. 2017; 292:21417–21430. DOI: 10.1074/jbc.M117.815639 [PubMed: 29074622]

28. Wilmes GM, Bell SP. The B2 element of the Saccharomyces cerevisiae ARS1 origin of replication requires specific sequences to facilitate pre-RC formation. Proc Natl Acad Sci U S A. 2002; 99:101–106. DOI: 10.1073/pnas.012578499 [PubMed: 11756674]

Europe PMC Funders Author Manuscripts

Europe PMC Funders Author Manuscripts

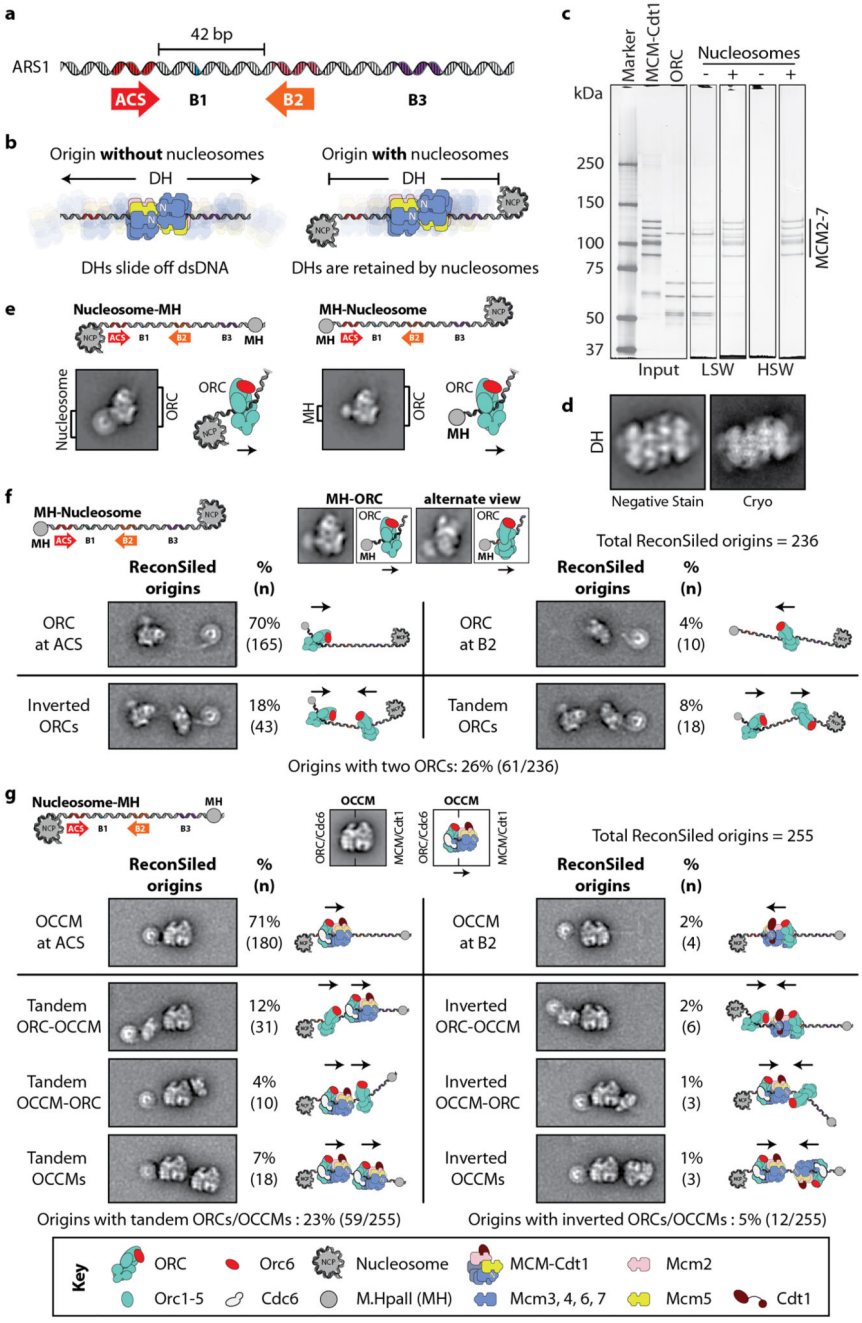


**Figure 1.** ***In silico*** **reconstitution of MCM recruitment to origins.**

**(a)** Linear structure of the ARS1 origin of replication in yeast. ACS and B2 are inverted high and low affinity binding sites for ORC. **(b)** Schematic representation of DH capture on DNA using nucleosomes as roadblocks. **(c)** Nucleosomes work as roadblocks that prevent DH linear diffusion. Nucleosome decorated, but not naked ARS1 DNA substrates retain MCM particles after both low and high-salt washes (LSW and HSW, respectively) in a bead-based DNA pulldown assay. For gel source data, see Supplementary Fig. 1 **(d)** Loaded MCMs form DHs. **(e)** ORC complexes interact with the ARS1 ACS. 2D class averages of ORC

bound to asymmetric origins show ORC complexes average in close proximity to the ACS-proximal roadblock. In this and all subsequent panels, black arrows indicate the orientation of the ORC C-terminal, MCM-recruitment interface. **(f)** *In silico* reconstitution (ReconSil) of ORC binding to asymmetric origins shows multiple modes of ORC interaction. Representative reconstituted origins are shown with schematics indicating directionality of ORC binding. The frequency of each class of ORC binding event is indicated as a percentage of total origins analyzed (n=236) **(g)** *In silico* reconstitution as in (f) showing MCM recruitment to origins in ATPγS (n=255).



Europe PMC Funders Author Manuscripts

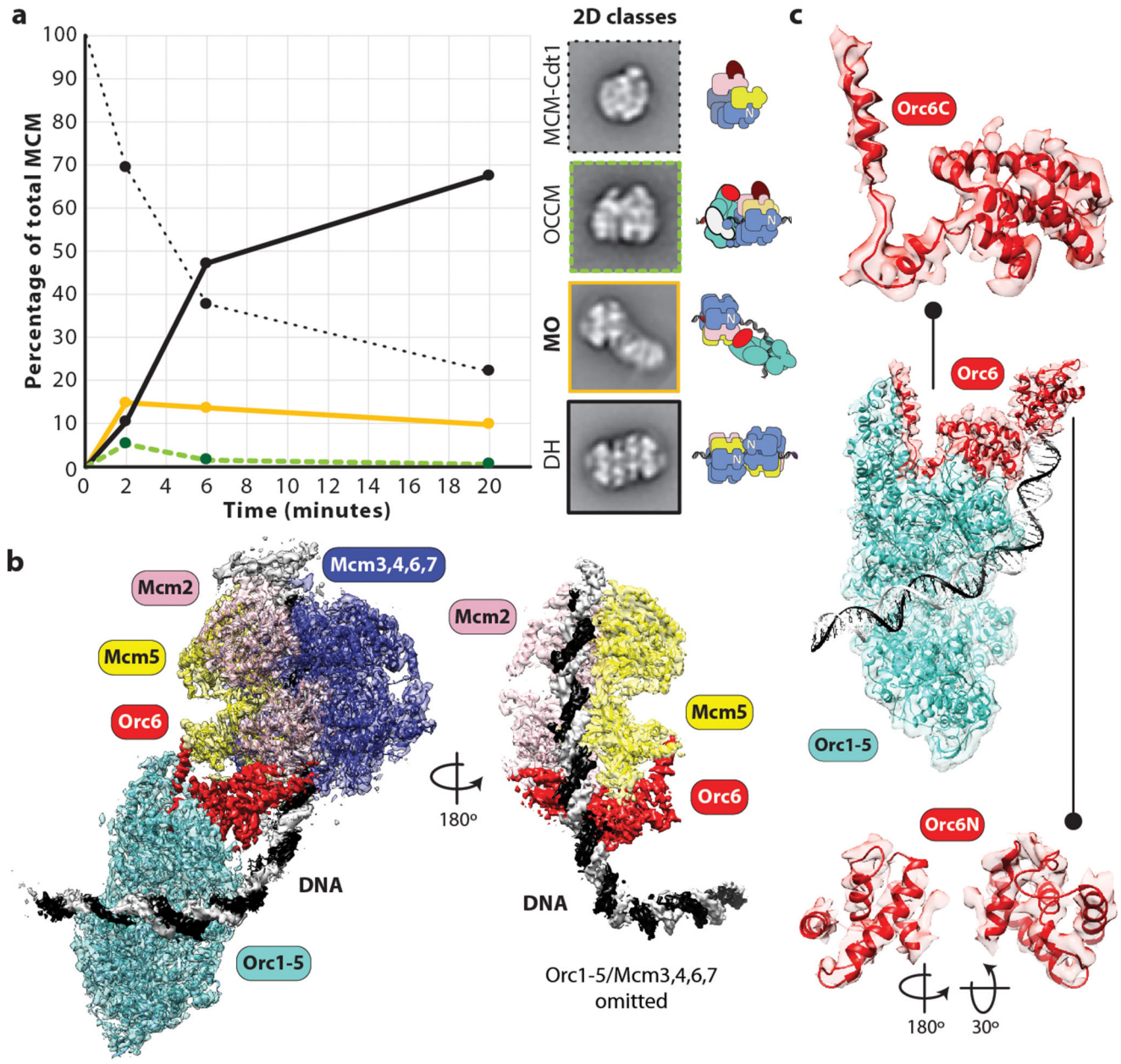


**Figure 2. Time-resolved helicase loading experiments lead to the identification of a new MCM loading intermediate.**

**(a)** A helicase loading time course analyzed by NS EM shows that the proportion of MCM molecules in the loading-competent MCM-Cdt1 species decreases as the loaded DH count increases. At 2 minutes, the OCCM loading intermediate peaks. At the same time, a second loading intermediate, evidently containing MCM and ORC (MO) can be identified. **(b)** Cryo-EM structure and atomic model of the MO intermediate. The model was obtained by real-space refining docked coordinates of MCM (PDB: 6EYC[24]), ORC (PDB: 5ZR1[18]) and an N-terminal Orc6 homology model. Orc6 (red) bridges Orc1-5 and MCM, contacting the N-terminal face of MCM and latching across the A domains of Mcm2 and Mcm5. MCM

and ORC are DNA-bound, spanning more than half of the ARS1 origin sequence; the DNA is bent and solvent exposed in-between the ORC and MCM complexes. **(c)** Views of N-terminal and C-terminal Orc6 in the context of the ORC complex.



Europe PMC Funders Author Manuscripts

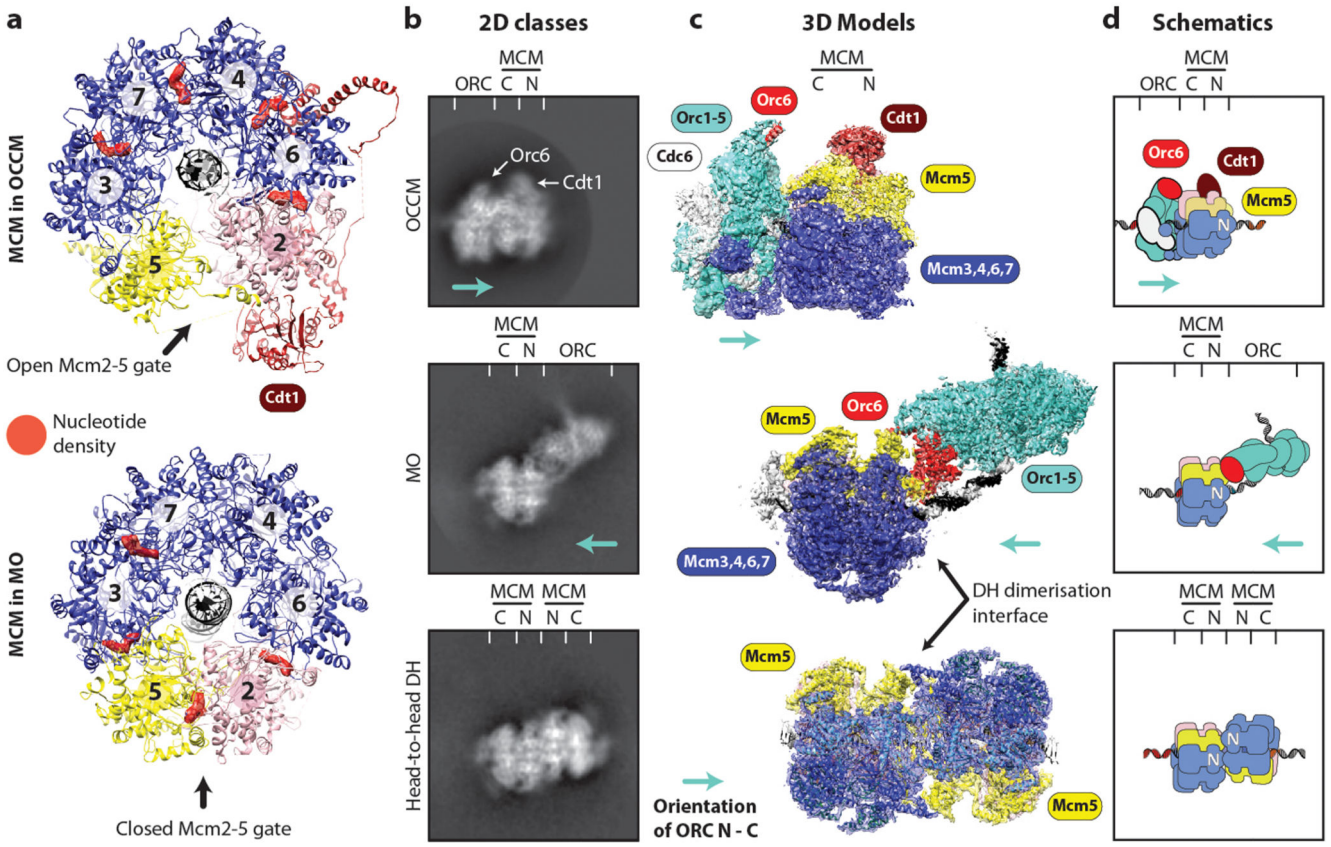


**Figure 3. The MO intermediate contains a post-catalytic closed MCM ring.**

**(a)** MCM in OCCM contains a notched ring with an opening spanning the near-entirety of Mcm2 and Mcm5[17]. ATPase interfaces at Mcm3-7, 7-4, 4-6 and 6-2 are ATPγS-bound in the OCCM structure. MCM in MO contains a closed Mcm2-5 gate. As observed in the post-catalytic DNA-loaded DH[7], nucleotide density (likely ADP) can be found at the Mcm6-2, 2-5, 5-3 and 3-7 ATPase interfaces. Cryo-EM 2D classes **(b)** 3D structures **(c)** and schematics **(d)** comparing the OCCM, MO and DH assemblies. In OCCM (top panels), the C-terminal domains of ORC and MCM form the interaction interface and both Cdc6 and Cdt1 are present. In MO (middle panels), ORC binds to the N-terminal dimerisation interface of MCM through Orc6. Cdc6 and Cdt1 are absent. The DH (bottom panels) forms a head-to-head, symmetrical dimer through interactions between its N-terminal domains.




Europe PMC Funders Author Manuscripts

Europe PMC Funders Author Manuscripts

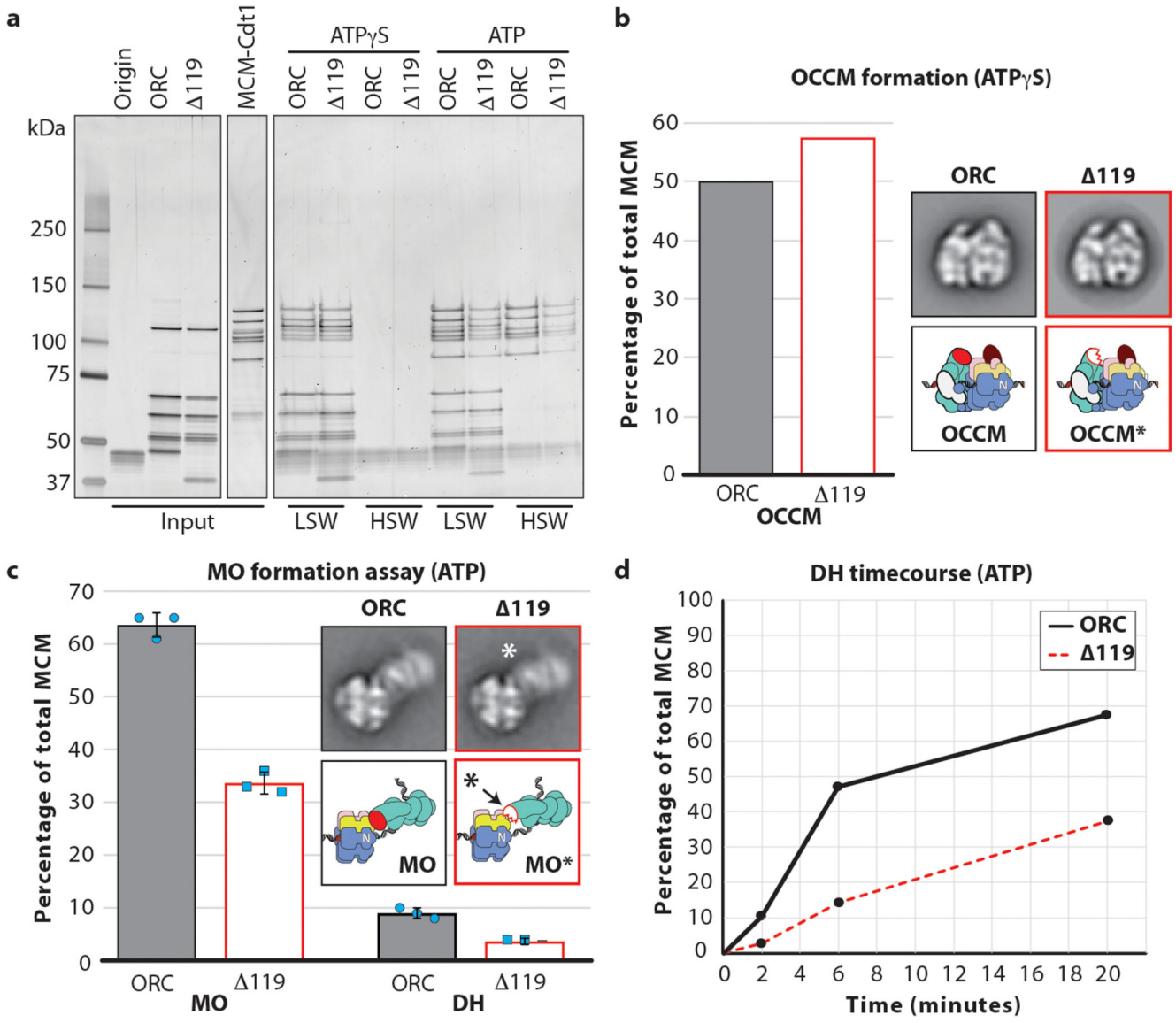


**Figure 4. N-terminal Orc6 truncation affects MCM loading but not recruitment.**

**(a)** a bead-based DNA pulldown assay demonstrates that ORC-OrcΔ119 (‘Δ119’) recruits MCM in ATPγS as efficiently as wild type ORC, however is less efficient at MCM loading, as observed both in low and high-salt wash conditions. For gel source data, see Supplementary Fig. 1. **(b)** According to negative stain EM experiments, OCCM formation is as efficient for Δ119 as it is for wild type ORC. **(c)** Efficiency of MO formation drops by ~50% when using Δ119 instead of wild type ORC. Efficiency of DH formation decreases by more than half. Bar chart shows mean ± standard deviation, n=3 independent experiments. *Negative stain 2D classes of MO containing wild type and Δ119 show a subtle change in ORC orientation (best appreciated in Supplementary Video 3). **(d)** In an EM-based time course experiment, DH formation dramatically slows when using Δ119 instead of wild type ORC.

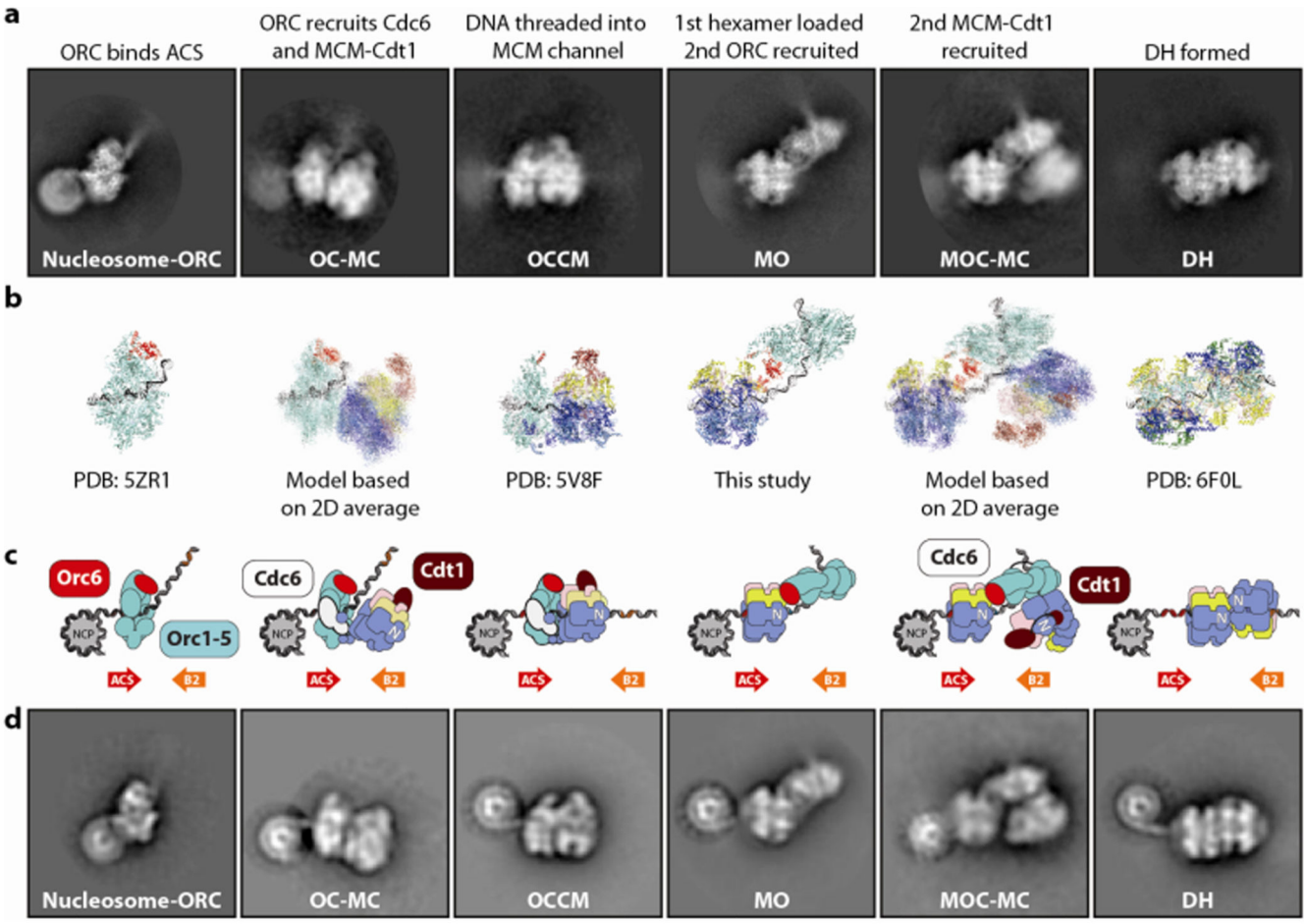


**Figure 5. The MCM double hexamer loading reaction visualized by EM.**

**(a)** Cryo-EM 2D averages of ORC at ACS (next to a nucleosome) indicate that DNA is bent as it traverses ORC; first MCM association with ORC before and after MCM threading; after first MCM loading, a second ORC binding event occurs at the N-terminal face of MCM; this ORC recruits a second MCM via the same mechanism as the first (OC-MC-like) and is poised for DH formation; finally the DH is formed around DNA. **(b)** The same reaction represented with atomic models or noisy projections for models generated from 2D averages, or with **(c)** cartoons. **(d)** The same six frames visualized by negative staining and ReconSil, showing the relative position of an ACS-flanking nucleosome to each of the licensing intermediates formed during first and second MCM hexamer recruitment and loading events.




Europe PMC Funders Author Manuscripts